THE JOURNAL OF PHYSICAL CHEMISTRY C

Article

pubs.acs.org/JPCC

Size-Dependent Mie's Scattering Effect on TiO_2 Spheres for the Superior Photoactivity of H_2 Evolution

Hua Xu,[†,‡,§] Xiaoqing Chen,[†,‡,§] Shuxin Ouyang,[‡] Tetsuya Kako,[†,‡] and Jinhua Ye*[,†,‡,§,∥]

[†]Graduate School of Chemical Science and Engineering, Hokkaido University, Sapporo 060-0814, Japan

[‡]Environmental Remediation Materials Unit, National Institute for Materials Science (NIMS), 1-2-1 Sengen, Tsukuba, Ibaraki 305-0047, Japan

[§]International Center for Materials Nanoarchitectonics (WPI-MANA), National Institute for Materials Science (NIMS), 1-2-1 Sengen, Tsukuba, Ibaraki 305-0047, Japan

[∥]Tu–NIMS Joint Research Center, School of Materials Science and Engineering, Tianjin University, 92 Weijin Road, Nankai District, Tianjin 300072, P.R. China

ABSTRACT: A novel strategy of coupling Mie's scattering effect into the light-absorption region of TiO_2 was developed to enhance the photocatalytic performance of H_2 evolution over TiO_2 spheres. The TiO_2 spheres with different diameters (330–750 nm) were controllably fabricated via adopting different sized polymer poly(methyl methacrylate) (PMMA) templates. The UV–visible absorption and reflectance spectra were employed for studying the absorption and scattering properties of these TiO_2 spheres. It was found that the scattering resonant peaks that indicate the strongly efficient scattering in different wavelength regions were largely dependent on the sizes of the TiO_2 spheres. The scattering resonant peaks have been detected around 366, 400, and 440 nm for the TiO_2 spheres with diameters of 380, 450, and 600 nm, respectively. Moreover, the photocatalytic efficiency of the H_2 evolution was found to be dependent on the size of the TiO_2 spheres. Among them, the TiO_2 spheres with a diameter of 380 nm exhibited the highest photocatalytic activity (313 μmol/(h·m^2)), about 5 times and 3 times of that of 330 and 450 nm sized TiO_2 spheres, respectively. The highest activity observed on 380 nm sized TiO_2 may be attributed to its optimized diameter, which can result in a highly efficient scattering effect in the light-absorption region of TiO_2 (λ < 387 nm).

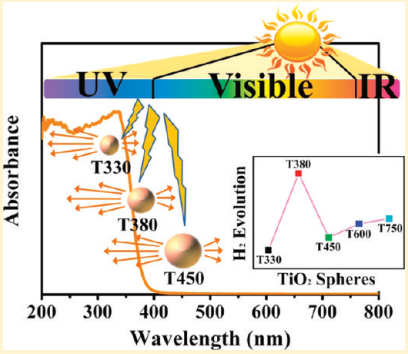

INTRODUCTION

Photocatalysis is an environmentally friendly and promising technology to convert solar energy into chemical energy.[1−5] In 1972, Fujishima and Honda reported that TiO_2 electrode could photocatalytically split water into H_2 and O_2 under some bias potential and UV light irradiation. After that, much work has been carried out on TiO_2 to enhance the photocatalytic activity.[6] In order to achieve this goal, the extensive efforts have been mainly focused on three aspects. One is the modification of the electronic structure to extend the light-absorption region, such as a series of anion doped TiO_2.[7−13] The other way is to fabricate single-crystalline TiO_2 with high-surface-energy crystal facets exposed[14−17] or mesoporous TiO_2 with large surface area,[18] which can offer more active sites during the photocatalytic reaction process. Third, improving the light utilization efficiency via the spatial structuring control (e.g., semi-hollow spheres) is also an effective method, but the relevant study is very limited.[19]

In general, the TiO_2 photocatalytic cycle comprises three steps: first, light excitation induces the transition of electrons from valence band to the conduction band, leaving an equal number of vacant sites (holes); second, the excited electrons and holes migrate to the surface of TiO_2; third, they react with the adsorbed electron donors and electron acceptors, respectively. Since the first step for the photocatalysis is the light excitation process, a high-efficient utilization of the incident light is an effective method to enhance the photocatalytic performance. Light can be scattered and redirected in many directions. Particularly, when the size of the particles is comparable to the wavelength of the incident light, the Mie's scattering happens. In the atmosphere, the clouds appear white, attributing to the Mie's scattering effect, which can scatter all wavelength of the visible light by the various sized dusts. If we introduce the Mie's scattering phenomenon into the TiO_2 spheres, when the light collides with the TiO_2 sphere with size comparable to its wavelength, the light scatters strongly along the forward direction. This scattering produces a pattern like an antenna lobe, with a sharper and more intense forward lobe (Scheme 1a).[20] Therefore, the path length of the incident light between the neighbored spheres will be increased,[21] leading to a promoted light utilization efficiency over the TiO_2 spheres. The scattering phenomenon has been applied in the dye-sensitized solar cells (DSSC) before;[22,23] however, to the best of our knowledge, there are few studies available on the light scattering effect over TiO_2 in the application of H_2 evolution. Previous work reported that the light scattering efficiency is largely dependent on the

Received: September 28, 2011
Revised: January 6, 2012
Published: January 9, 2012

   dx.doi.org/10.1021/jp209378t | J. Phys. Chem. C 2012, 116, 3833–3839

Scheme 1. Schematic Illustration of the Mie's Scattering Phenomenon among the TiO_2 Spheres (a) and the Simulated Scattering Region for the TiO_2 Spheres with Different Diameters (T330, T380, and T450 Represent the TiO_2 Spheres with Diameters of 330 nm, 380 nm, and 450 nm, Respectively) (b)

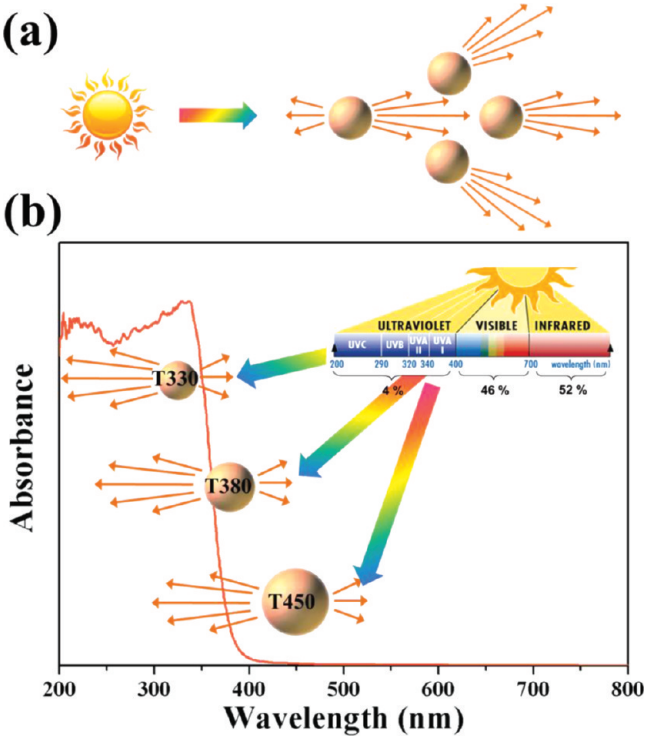

size of the scattering particle, and the wavelength of the incident light.[24] Therefore, fabrication of TiO_2 spheres with suitable diameter is critical to induce the Mie's scattering effect happening in the light absorption region of TiO_2.

In this work, we develop a strategy of coupling Mie's scattering into the light-absorption region of TiO_2 to enhance the light-utilization efficiency of the TiO_2 spheres. The band gap of TiO_2 is 3.2 eV, which can only be excited by the light with wavelength smaller than 387 nm. According to the Mie's scattering theory, the light will be strongly scattered on the surface of TiO_2 with an appropriate size comparable to its wavelength. When the scattering cross-section exhibits a number of resonances for a given particle size of TiO_2 sphere, the scattering will be very efficient at these wavelengths. Therefore, the scattering efficiency in different wavelength regions of the incident light spectrum is largely dependent on the diameter of TiO_2 spheres. Only when the scattering resonant peak, which indicates the strongly efficient scattering,[25] is coupled into the light-absorption region of TiO_2, the scattering and absorption for the TiO_2 is effective, followed with the highest light utilization efficiency. As shown in Scheme 1b, the scattering phenomenon occurs on the TiO_2 spheres with diameters of smaller (330 nm), comparable (380 nm), and larger (450 nm) than the light absorption edge of TiO_2 (about 387 nm) is depicted. We can assume that the scattering effect that happens on the TiO_2 spheres will be various and related to the different diameters. On the basis of the above assumption, herein, the TiO_2 spheres with different sizes (330 nm, 380 nm, 450 nm, 600 nm, and 750 nm) have been selectively fabricated. The scattering resonant peaks over the TiO_2 spheres were checked to study the correlation between the particle size and the scattering efficiency. The further photocatalytic H_2 evolution and photoelectrochemical measurements over the TiO_2 spheres were investigated to test the validity of the coupling strategy of the size-dependent Mie's scattering effect.

EXPERIMENTAL SECTION

Synthesis of TiO_2 Spheres. The TiO_2 spheres were prepared via a facile sol–gel method[26] by the coagulation of titanium tetra-*n*-butyl (TBOT) with the polymer poly(methyl methacrylate) (PMMA) spheres as templates. Typically, 0.05 g PMMA spheres and 0.6 mL ammonium were first added into a mixed solution of 75 mL of ethanol and 25 mL of acetonitrile. In this step, the PMMA spheres were negatively charged, while the ammonium was selected to electrostatically stabilize the PMMA template because of the positively charged NH_4^+. After being stirred for 20 min, 3 mmol of TBOT was subsequently added and adsorbed on the surface of the NH_4^+/$PMMA^-$ spheres, followed with a series of hydrolysis processes to form the amorphous TiO_2 via magnetic stirring at room temperature for 24 h. Finally, the white precipitation was heated at 500 °C for 2 h with a temperature ramping rate of 1 °C/min, all the PMMA polymers were removed, leading to the formation of TiO_2 hollow spheres. By using different sized PMMA spheres as the template, TiO_2 spheres with different diameters were selectively prepared. The diameters of the TiO_2 spheres were controlled to be 330, 380, 450, 600, and 750 nm (denoted as T330, T380, T450, T600, and T750) by adopting 170, 260, 330, 450, and 670 nm sized PMMA spheres, respectively.

Preparation of TiO_2 Films. The TiO_2 films used for the photoelectrochemical test were prepared via a spin-coating method. The 20 mg of TiO_2 samples were first dispersed into 10 mL of ethanol solvent by ultrasonic treatment, then spin-coated on the ITO substrate layer by layer for 50 times. In the procedure of spin coating, every drop of the TiO_2 suspension was about 0.05 mL. In each cycle, 3 drops of suspension was dripped on the ITO substrate. The spin speed and time were 800 rpm for 5 s followed with 1000 rpm for 30 s. Finally, the coated films were heated to 500 °C at a rate of 1 °C/min and kept at this temperature for 2 h.

Characterization. The X-ray diffraction (XRD) patterns of the prepared samples were conducted on a Rigaku Multiflex diffractometer (RINT 2000; Rigaku Corp., Japan) with monochromatized Cu Ka radiation (λ=1.54178 Å). The size and morphology of the samples were observed by a scanning electron microscope (SEM, JSM-6701F, JEOL Co., Japan) and transmission electron microscope (TEM, JEM-200 CX, JEOL Co., Japan) operating at 200 kV. The Brunauer–Emmett–Teller (BET) surface areas were recorded by a surface area analyzer (Tristar 3000, Micromeritics Inc., USA) with nitrogen absorption at 77 K. The UV–visible diffuse reflectance spectra were measured on a UV–visible spectrophotometer (UV-2500PC, Shimadzu Co., Japan).

Photocatalytic H_2 Evolution Process. Photocatalytic reactions of H_2 evolution were carried out in a closed gas circulation system with an external-irradiation Pyrex-cell. The light source was a 300 W xenon lamp. The intensity of the light at 300–800 nm was measured to be 242.3 mW/cm^2 using a spectroradiometer (USR-40; Ushio Inc., Japan). The cocatalyst Pt was loaded by an in situ photodeposition method. The 0.5 wt % Pt-loaded catalyst (0.09 g) was first ultrasonically dispersed into monodispersed spheres suspended in a methanol aqueous solution (50 mL of methanol and 220 mL of water).

dx.doi.org/10.1021/jp209378t | J. Phys. Chem. C 2012, 116, 3833–3839

Then, magnetic stirring was used to stabilize the suspension during the whole photocatalytic H_2 evolution process. The evolved gas including H_2 was analyzed by an online gas chromatograph (GC-8A; Shimadzu Corp., Japan) equipped with a thermal conductivity detector.

Photoelectrochemical Measurement. Photocurrent measurements were performed with an electrochemical station (ALS/CH model 650A, Japan) using a three-electrode mode with 0.1 M Na_2SO_4 solution as the electrolyte. The TiO_2 photoanodes were used as working electrodes; a Pt wire served as a counter electrode. The Ag/AgCl electrode was used as the reference electrodes. The illumination source was a 500 W Xe lamp (Optical ModuleX; Ushio Inc., Japan). The intensity of the light at 300−800 nm was measured to be 140.4 mW/cm^2 using a spectroradiometer (USR-40; Ushio Inc., Japan). In the photocurrent−time measurement, the TiO_2 photoelectrodes were illuminated at normal incidence of light through a quartz window. The voltage-scan speed was 0.1 V/s, and light was chopped manually at regular intervals.

RESULTS AND DISCUSSION

The XRD patterns of the as-prepared TiO_2 samples are shown in Figure 1. The XRD profiles of all the samples can be

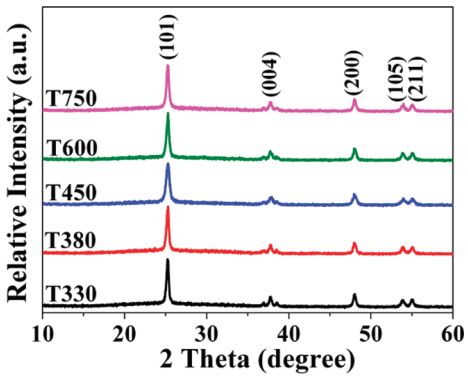

Figure 1. XRD patterns of the as-prepared TiO_2 spheres.

coincidently indexed by the standard anatase TiO_2 pattern (JCPDS file No. 71−1167). The peaks at 25.25, 37.72, 48.03, 53.91, and 54.99 degree can be assigned to (101), (004), (200), (105), and (211) crystal planes of anatase TiO_2, respectively. Meanwhile, the average crystallite sizes of the TiO_2 samples were calculated by the Scherrer's formula: $D = K\lambda/\beta \cos\theta$, where λ was the wavelength of the X-ray radiation (λ = 0.15418 nm), K was the Scherrer constant (K = 0.89), θ was the position of X-ray diffraction peak, and β was the full width at half-maximum (fwhm) of the (101) plane for anatase TiO_2. The calculated sizes are 22.8, 25.6, 22.1, 21.2, and 22.3 nm for T330, T380, T450, T600, and T750, respectively. Therefore, the crystallinity for all the TiO_2 samples is not obviously different. It is well-known that the crystallinity of the TiO_2 during the crystal growth process is largely dependent on the water content, the solution acidity, and the calcination temperature. Since the TiO_2 spheres were prepared in the same procedure and similar preparation environment (0.06 mL ammonium added and calcination at 500 °C for 2 h), thus leading to the similar crystallinity for all the TiO_2 samples.

The size and morphology of the TiO_2 samples can be observed by the SEM images (Figure 2a−e). There is no obvious difference in the surface morphology except for the size among the TiO_2 spheres with different diameters around 330, 380, 450, 600, and 750 nm, respectively. Furthermore, the TEM image confirms the spherical structure with an average size of 380 nm for T380 (Figure 2f). Meanwhile, the contrast between the bold dark ring and the bright inner circle indicates that the sphere is hollow, which is resulted from the removal of the PMMA template via calcination. The enlarged representative surface of the TiO_2 sphere (Figure 2g) reveals that the TiO_2 sphere consists of a large amount of tiny nanoparticles (~3 nm). The spacing of the lattice fringes is 0.350 nm as shown in the HRTEM image (Figure 2h), which is associated with the (101) lattice plane of the anatase TiO_2.

As shown in Figure 3, the N_2 adsorption−desorption isotherms of T380 exhibit a typical Type IV isotherm with a hysteresis loop, which is associated with capillary condensation taking place in mesopores, and the limiting uptake over a range of high P/P_0.[27] Moreover, the pore-size distribution curve of T380 (inset of Figure 3) indicates that the TiO_2 samples contain mesopores with diameter smaller than 10 nm, this result is well consistent with the TEM image as shown in Figure 2g. The TiO_2 spheres are made of large amounts of small nanoparticles and the mesopores are resulted from the aggregates of the nanoparticles. Therefore, besides the contribution of the external and internal surface areas of the hollow sphere, the pores resulting from the aggregation of the small TiO_2 nanocrystalline consisting in the TiO_2 sphere also make an effort to the total surface area. Finally, the Brunauer−Emmett−Teller (BET) specific surface areas are recorded as 13.8, 9.4, 10.1, 10.2, and 8.8 m^2/g for T330, T380, T450, T600, and T750, respectively (as listed in Table 1).

The optical properties of the TiO_2 sphere powders are shown in Figure 4. All the TiO_2 samples exhibit the similar light absorption edge around 380 nm (Figure 4a), while little differences exist in the reflectance spectra, especially in the region of 335−370 nm (inset of Figure 4b), which reveals that T380 presents a relatively higher reflectance intensity compared with other TiO_2 samples. It is well-known that the light-scattering performance of TiO_2 is strongly dependent on the particle size, and the size dependency of the scattering effect can be evaluated by the reflectance spectra to some extent.[28] Therefore, since T380 exhibits the strongest reflectance intensity in the region of 335−370 nm, it might have a strong scattering efficiency in this region.

The photocatalytic activities of the H_2 evolution were tested for all the TiO_2 sphere samples. The amounts of the evolved H_2 over the TiO_2 samples were 76, 265, 94, 136, and 131 μmol/h for T330, T380, T450, T600, and T750, respectively (as depicted in Table 1). Among which, T380 exhibited obviously higher photocatalytic activity compared with the other TiO_2 samples. Usually the photocatalytic performance of TiO_2 is affected by various factors such as the morphology, the phase composition, the crystallinity, the surface area, and so on. In this work, considering that the crystallinity is not appreciably different for these TiO_2 samples (Figure 1), the effect of the crystallinity on the photocatalytic performance can be ignored. Moreover, taking the surface area into account, the photocatalytic activities of the TiO_2 samples are 61, 313, 103, 148, and 165 μmol/(h·m^2) for T330, T380, T450, T600, and T750, respectively (Figure 5), in which the photoactivity of T380 is also superior to that of other TiO_2 samples. Therefore, the highest photocatalytic activity of the H_2 evolution over T380 can be attributed to the fact that the unique diameter can result in a strongly efficient scattering effect in the light absorption

dx.doi.org/10.1021/jp209378t | J. Phys. Chem. C 2012, 116, 3833−3839

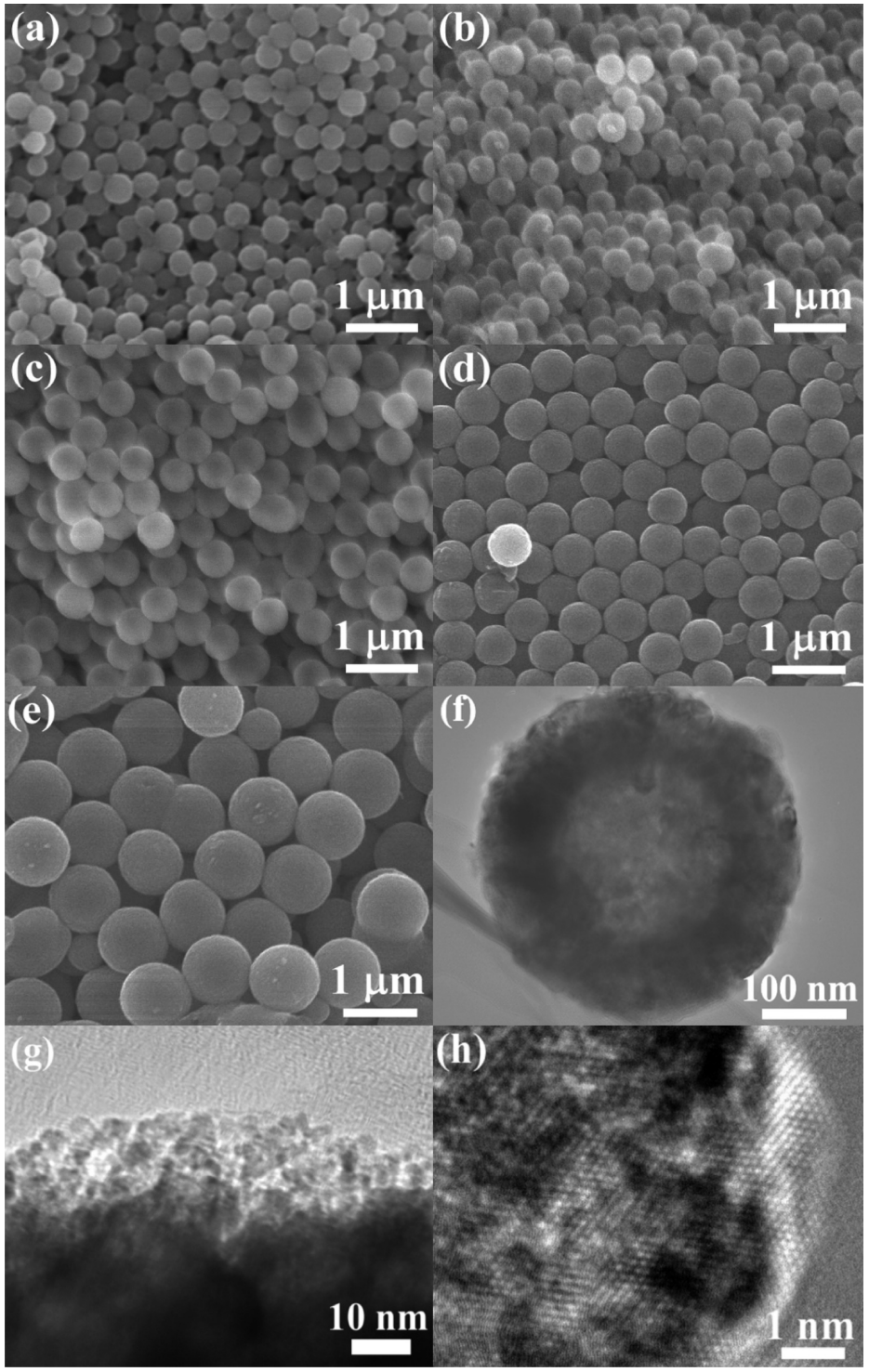

Figure 2. SEM images of the TiO_2 spheres, (a) T330, (b) T380, (c) T450, (d) T600, and (e) T750; the TEM image (f), the high-magnified TEM image (g), and HRTEM image (h) of T380.

region of TiO_2 and thus lead to the enhanced photocatalytic performance.

The strong scattering effect is largely dependent on the particle size, which can be theoretically explained as follows. When the size of sphere is comparable to the incident-light wavelength, the Mie's scattering occurs. Theoretically, the scattered wave is found to be necessary to obtain the right boundary conditions between incident wave and the field inside the sphere. For an incident light wavelength λ, the scattering behavior of a system, which consists of dispersed spherical particles, can be fully described by the radius of sphere r and the complex refractive index m. The complex Mie coefficients a_n and b_n can be deduced by the complex Bessel–Riccatti functions ψ and ζ

$$a_n = \frac{\psi'_n(mx)\psi_n(x) - m\psi_n(mx)\psi'_n(x)}{\psi'_n(mx)\zeta_n(x) - m\psi_n(mx)\zeta'_n(x)}$$

dx.doi.org/10.1021/jp209378t | J. Phys. Chem. C 2012, 116, 3833–3839

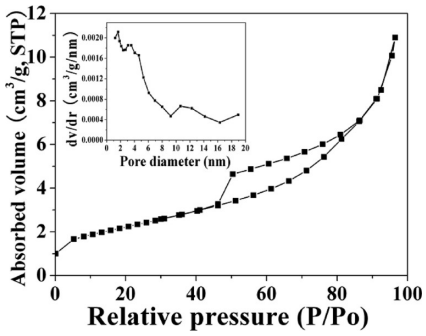

Figure 3. Nitrogen adsorption−desorption isotherms and pore-size distribution curve (inset) of the prepared TiO_2 sample(T380).

Table 1. BET Surface Areas, Photocatalytic Activities, and Photoelectrochemical Properties of the As-Prepared TiO_2 Spheres

	T330	T380	T450	T600	T750
BET surface area (m^2/g)	13.8	9.4	10.1	10.2	8.8
amounts of H_2 evolution (μmol/h)	76	265	94	136	131
photocurrent density ($\mu A/cm^2$)	14.9	59.2	36.9	13.0	9.2

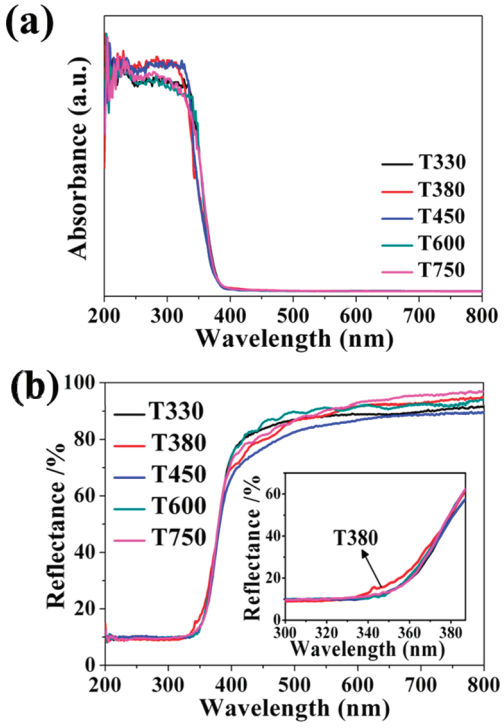

Figure 4. (a) UV−visible absorption spectra of the TiO_2 powders; and (b) the UV−visible diffuse reflectance spectra of the TiO_2 powders and the enlarged part in the region of 300−387 nm (inset).

$$b_n = \frac{m\psi'_n(mx)\psi_n(x) - \psi_n(mx)\psi'_n(x)}{m\psi'_n(mx)\zeta_n(x) - \psi_n(mx)\zeta'_n(x)}$$

where the size parameter x is taken as $x = 2\pi r/\lambda$.

The Mie coefficients a_n and b_n are functions with numerous poles in the complex plane. The scattering, absorption, and

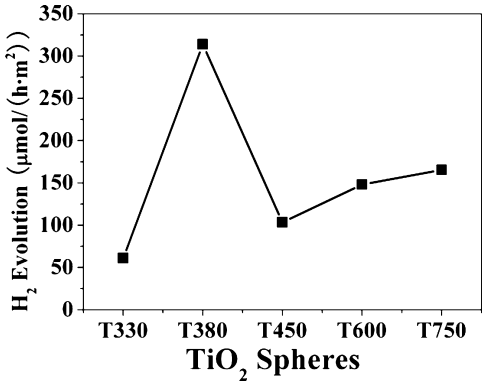

Figure 5. Photocatalytic activities of H_2 evolution over the different sized TiO_2 spheres (with 0.5 wt % Pt loaded) under UV−visible light irradiation (λ > 300 nm).

extinction efficiencies are given by

$$Q_{sca} = \frac{2}{x^2}\sum_{n=1}^{\infty}(2n+1)(|a_n|^2 + |b_n|^2)$$

$$Q_{abs} = Q_{ext} - Q_{sca}$$

$$Q_{ext} = \frac{2}{x^2}\sum_{n=1}^{\infty}(2n+1)\mathrm{Re}(a_n + b_n)$$

Therefore, the scattering cross-section exhibits a number of resonances for a given particle size; at these wavelengths, the scattering is very efficient.[29,30]

To verify the existence of the scattering effect in the H_2 evolution process, the TiO_2 suspensions obtained after the H_2 evolution test were used to check the scattering resonant peaks by the UV−visible reflectance spectra from 300 to 800 nm.[25,31] As shown in Figure 6, the experimental results reveal that the

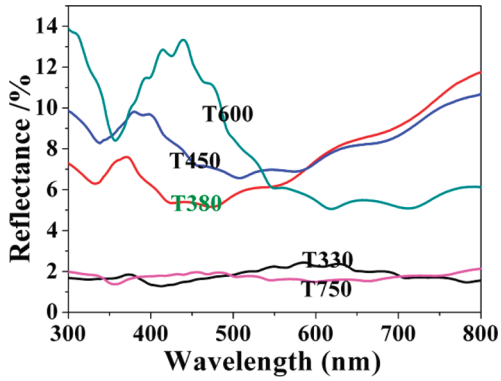

Figure 6. UV−visible reflectance spectra of the TiO_2 suspensions obtained after the H_2 evolution test to detect the scattering resonant peaks of the TiO_2 spheres.

scattering effect for the various sized TiO_2 spheres in the incident light spectrum are obviously different. The TiO_2 sample with a diameter of 380 nm exhibits the strong resonant peak around 366 nm, indicating that the incident light strongly scatters on the 380 nm sized TiO_2 sphere at wavelength around 366 nm. The scattered light then transfers to and is absorbed by the neighbored spheres, thus inducing more photoexcited electrons to reduce the H^+ ions into H_2 molecules. For TiO_2 spheres, only for the light with wavelengths shorter than the

dx.doi.org/10.1021/jp209378t | J. Phys. Chem. C 2012, 116, 3833−3839

absorption edge (λ < 387 nm), scattering and absorption is effective. As for the TiO_2 spheres with diameters of 450 and 600 nm, the peaks of scattering resonances locate at 400 and 440 nm, thus the scattering effects are relatively limited to the enhancement of light absorption for TiO_2. For the 750 nm sized TiO_2 sample, a very weak and broad peak between 350 and 600 nm can be detected with careful observation. The weak scattering resonance peak might be attributed to the low scattering coefficient reported by Thiele and his co-workers.[32] In the photocatalytic H_2 evolution process, more light can be absorbed by the TiO_2 samples, more electrons will be excited and take part in the H^+ reduction reaction, thus lead to a higher H_2 output efficiency. Since the TiO_2 sample with a diameter of 380 nm exhibits the strong effective scattering effect in the light-absorption region of TiO_2, more light will be scattered and absorbed by the TiO_2, thus the light utilization efficiency will be largely enhanced followed with the superior photocatalytic activity, which is well in accordance with our photocatalytic tests that T380 showed the higher photocatalytic activity of H_2 evolution compared with other TiO_2 samples (T330, T450, T600, and T750). In conclusion, only the scattering and absorption that happened in the light absorption region of TiO_2 can make a great contribution to the effective light-utilization efficiency followed with the enhancement of photocatalytic performance.

In order to further confirm that the photon-to-electron conversion efficiency of the TiO_2 sphere is affected by the size-dependent Mie's scattering effect, the photoelectrochemical measurements of the TiO_2 photoanodes have been conducted. Figure 7a shows the photocurrent−time (I−t) curves measured with a three-electrode mode and 0.1 M Na_2SO_4 solution as the electrolyte. Under a bias potential of 0.6 V, the photocurrent densities of the TiO_2 spheres are 14.9, 59.2, 36.9, 13.0, and 9.2 $\mu A/cm^2$ for T330, T380, T450, T600, and T750, respectively, in which the photocurrent intensity of T380 is the highest (Figure 7b), indicating that T380 has the best photon-to-electron conversion efficiency. This result is consistent with the results from the photocatalytic H_2 evolution tests. In the photocatalytic H_2 evolution process, the photoexcited electrons will reduce the protons (H^+) into H_2, thus an enhanced light-utilization efficiency followed with the better photon-to-electron conversion performance might result in a superior output efficiency of H_2.

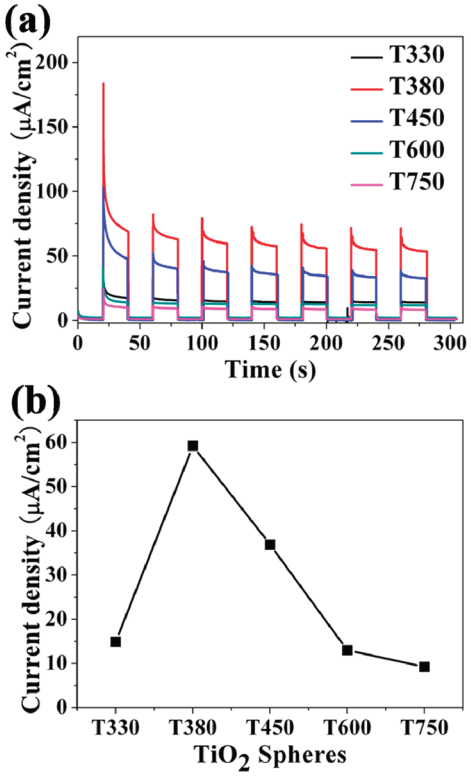

Figure 7. (a) Photocurrent curves (I−t) of the as-prepared TiO_2 photoanodes measured under UV−visible light irradiation (λ > 300 nm); (b) the comparison of the photoelectrochemical properties of the TiO_2 thin films samples.

CONCLUSIONS

In summary, the Mie's scattering effect was introduced into the application of photocatalytic H_2 evolution over TiO_2 spheres. TiO_2 spheres with different diameters (330−750 nm) were fabricated to investigate the correlation between the particle size and the scattering effect. In contrast to the 450 and 600 nm sized TiO_2 spheres, the TiO_2 with a diameter of 380 nm exhibited the strong efficient scattering effect in the light absorption region of TiO_2, thus leading to a higher light-utilization efficiency, followed with a considerable enhancement of the photocatalytic activity. This study proposes a novel strategy that coupling the effect of Mie's scattering into the light absorption region of TiO_2 via morphological modulation can improve the photocatalytic performance in the H_2 evolution. Moreover, it will provide a potential and promising approach to effectively enhance the light utilization efficiency for other semiconductor photocatalysts, especially for the visible-light-driven photocatalysts with the optimized diameter.

AUTHOR INFORMATION

Corresponding Author

*Tel: (+81)-29-859-2646. E-mail: Jinhua.Ye@nims.go.jp.

ACKNOWLEDGMENTS

This work was partially supported by the World Premier International Research Center Initiative (WPI Initiative) on Materials Nanoarchitectonics and the MEXT Program for Development of Environmental Technology using Nanotechnology.

REFERENCES

(1) Tong, H.; Ouyang, S. X.; Bi, Y. P.; Umezawa, N.; Oshikiri, M.; Ye, J. H. *Adv. Mater.* **2012**, *24*, 229.
(2) Hoffmann, M. R.; Martin, S. T.; Choi, W. Y.; Bahnemann, D. W. *Chem. Rev.* **1995**, *95*, 69−96.
(3) Linsebigler, A. L.; Lu, G. Q.; Yates, J. T. *Chem. Rev.* **1995**, *95*, 735−758.
(4) Zou, Z. G.; Ye, J. H.; Sayama, K.; Arakawa, H. *Nature* **2001**, *414*, 625−627.
(5) Ouyang, S. X.; Ye, J. H. *J. Am. Chem. Soc.* **2011**, *133*, 7757−7763.
(6) Fujishima, A.; Honda, K. *Nature* **1972**, *238*, 37.
(7) Asahi, R.; Morikawa, T.; Ohwaki, T.; Aoki, K.; Taga, Y. *Science* **2001**, *293*, 269−271.
(8) Hensel, J.; Wang, G. M.; Li, Y.; Zhang, J. Z. *Nano Lett.* **2010**, *10*, 478−483.
(9) Zhao, W.; Ma, W. H.; Chen, C. C.; Zhao, J. C.; Shuai, Z. G. *J. Am. Chem. Soc.* **2004**, *126*, 4782−4783.
(10) Tang, J. W.; Cowan, A. J.; Durrant, J. R.; Klug, D. R. *J. Phys. Chem. C* **2011**, *115*, 3143−3150.
(11) Yu, J. C.; Yu, J. G.; Ho, W. K.; Jiang, Z. T.; Zhang, L. Z. *Chem. Mater.* **2002**, *14*, 3808−3816.

(12) Ren, W. J.; Ai, Z. H.; Jia, F. L.; Zhang, L. Z.; Fan, X. X.; Zou, Z. G. *Appl. Catal. B* **2007**, *69*, 138−144.
(13) Yu, J. C.; Ho, W. K.; Yu, J. G.; Yip, H.; Wong, P. K.; Zhao, J. C. *Environ. Sci. Technol.* **2005**, *39*, 1175−1179.
(14) Yang, H. G.; Sun, C. H.; Qiao, S. Z.; Zou, J.; Liu, G.; Smith, S. C.; Cheng, H. M.; Lu, G. Q. *Nature* **2008**, *453*, 638−641.
(15) Liu, S. W.; Yu, J. G.; Jaroniec, M. *J. Am. Chem. Soc.* **2011**, *23*, 4085−4093.
(16) Ahmed, A. Y.; Kandiel, T. A.; Oekermann, T.; Bahnemann, D. *J. Phys. Chem. Lett.* **2011**, *2*, 2461−2465.
(17) Zheng, Z. K.; Huang, B. B.; Qin, X. Y.; Zhang, X. Y.; Dai, Y.; Jiang, M. H.; Wang, P.; Whangbo, M. H. *Chem.—Eur. J.* **2009**, *15*, 12576−12579.
(18) Schattka, J. H.; Shchukin, D. G.; Jia, J.; Antonietti, M.; Caruso, R. A. *Chem. Mater.* **2002**, *14*, 5103−5108.
(19) Li, H. X.; Bian, Z. F.; Zhu, J.; Zhang, D. Q.; Li, G. S.; Huo, Y. N.; Li, H.; Lu, Y. F. *J. Am. Chem. Soc.* **2007**, *129*, 8406−8407.
(20) Mie, G. *Ann. Phys.* **1908**, *330*, 377−445.
(21) Koo, H. J.; Park, J.; Yoo, B.; Yoo, K.; Kim, K.; Park, N. G. *Inorg. Chim. Acta* **2008**, *361*, 677−683.
(22) Wu, X.; Lu, G. Q.; Wang, L. Z. *Energy Environ. Sci.* **2011**, *4*, 3565−3572.
(23) Yu, I. G.; Kim, Y. J.; Kim, H. J.; Lee, C.; Lee, W. I. *J. Mater. Chem.* **2011**, *21*, 532−538.
(24) Usami, A. *Chem. Phys. Lett.* **1997**, *277*, 105−108.
(25) Retsch, M.; Schmelzeisen, M.; Butt, H. J.; Thomas, E. L. *Nano Lett.* **2011**, *11*, 1389−1394.
(26) Tang, F. Q.; Fudouzi, H.; Zhang, J. X.; Sakka, Y. *Scr. Mater.* **2003**, *49*, 735−740.
(27) Sing, K. S. W.; Everett, D. H.; Haul, R. A. W.; Moscou, L.; Pierotti, R. A.; Rouquerol, J.; Siemieniewska, T. *Pure Appl. Chem.* **1985**, *57*, 603−619.
(28) Bohren, C. F.; Huffman, D. R. Wiley: New York, 1983; pp 103−111.
(29) Scholz, S. M.; Vacassy, R.; Dutta, J.; Hofmann, H. *J. Appl. Phys.* **1998**, *83*, 7860−7866.
(30) Hulst, H. C. *Light Scattering by Small Particles*; Dover: New York, 1981.
(31) Ye, Q. L.; Yoshikawa, H.; Bandow, S.; Awaga, K. *Appl. Phys. Lett.* **2009**, *94*, 063114.
(32) Thiele, E. S.; French, R. H. *J. Am. Ceram. Soc.* **1998**, *81*, 469−479.